Microsyst Technol (2013) 19:53–60
DOI 10.1007/s00542-012-1610-1

TECHNICAL PAPER

Design and modeling of 2-D photonic crystals based hexagonal triple-nano-ring resonators as biosensors

Chong Pei Ho · Bo Li · Aaron J. Danner · Chengkuo Lee

Received: 6 February 2012 / Accepted: 1 June 2012 / Published online: 29 June 2012

Abstract Si photonic crystal resonator which comprises of three hexagonal nano-rings has been investigated. A forward-dropped peak at 1536.60 nm proves that the proposed triple nano-ring (TNR) resonator is a good channel drop filter, which makes it a good candidate for nanomechanical sensor applications. In this paper, the application of the TNR structure as a biosensor has been studied. It is realized that the symmetrical resonance output of the TNR resonator enhance its suitability as a biosensor as this characteristic makes sensing multiple biomolecules and corroboration of results at same input frequency possible.

1 Introduction

Photonic crystals (PhCs) are engineered nanostructures which provide capability of controlling and manipulating the propagation of electromagnetic waves within a given frequency range. A thin film of periodic dielectric nanostructures, e.g. an array of holes in a silicon slab, exhibits a photonic band gap (PBG) for certain frequency ranges. More clearly, the propagation of light within PBG frequency range is forbidden in PhC nanostructures. By leveraging the PBG effect, the light within the PBG frequency range can be guided or localized by introducing certain defects in the PhC structures (Hung-Ta et al. 2009). Cavity defects in two-dimensional (2-D) PhCs can provide a high degree of both spatial and temporal light confinement. Various microcavity or nanocavity based PhC resonators are demonstrated as ultra compact filters of high quality factor (Q-factor) (Vahala 2003; Lalanne et al. 2008). The PhCs based channel drop filters have been reported for applications in wavelength division multiplexer (WDM) communication systems (Zhang and Qiu 2005; Qiang et al. 2007; Monifi et al. 2009; Djavid et al. 2008; Saghirzadeh Darki and Granpayeh 2010). The ultimate sizes of such PhC filters are suggested to be less than 1/10,000 of those of conventional optical devices. On the other hand, the surface state variation and mechanical deformation of microcavity or nanocavity of PhC resonators and filters leads to measurable resonance wavelength shift. This unique feature makes PhC resonators and filters become good biochemical sensors and nanomechanical sensors (Lu et al. 2010; Lee and Thillaigovindan 2009; Lee et al. 2008).

Single hexagonal PhC ring resonator has been investigated as biochemical sensors and nanomechanical sensors (Hsiao and Lee 2010, 2011; Mai et al. 2011). Owning to good light confinement, the size of a hexagonal nano-ring resonator can be as small as 3 μm^2. 2-D PhCs based hexagonal dual nano-ring (DNR) resonators with appropriate spacing between the two rings can provide backward or forward channel drop, and wavelength selective channel drop (Li et al. 2011a, 2011b).

One major application of such channel drop enabled nano-ring resonators is the sensing and detection of biomolecules. As an avenue to enhance effectiveness, it is also greatly desired that multiple biomolecules can be sensed at the same time (Vos et al. 2009). In order to achieve this, designs including ring resonator or waveguides are often made into cascading repetitions or are placed into an array (Vos et al. 2009; Iqbal et al. 2010; Kirk et al. 2011). In such designs, it is important that the repeating units are isolated

C. P. Ho · B. Li · A. J. Danner · C. Lee (✉)
Department of Electrical and Computer Engineering, National University of Singapore, 4 Engineering Drive 3, Singapore 117576, Republic of Singapore
e-mail: elelc@nus.edu.sg

to avoid interference of results. This will cause possible constraints on the Q-factors as well as the size of the PhC structure. In addition, cascading designs often increases the complexity of the device, thus complicating fabrication and testing process.

In this work, we report the design and modeling of a hexagonal PhC lattice triple-nano-ring (TNR) resonator to be used as a biosensor and how its symmetric resonance output and add-drop channel characteristic can be harnessed to enable the detection of multiple biomolecules simultaneously. In addition, the TNR resonator biosensor is also equipped with a novel function to corroborate the results obtained by reversing the light input and the output. Similar concept of positioning particular biomolecules into specific holes in the PhC structure to induce refractive index changes has been realized experimentally (Intonti et al. 2009) and how this idea is harnessed in our design will be discussed in Sect. 3.

2 Design and characteristics of TNR resonator

The cavity mode derived by plane wave expansion (PWE) method in PhC slab structure has been reported in good agreement with the measured results (Kitamura et al. 2005). By using this PWE method, the band structure of a silicon PhCs slab with hexagonal lattice of holes is derived and shown in Fig. 1. A PhC slab of 220 nm thick silicon layer on the 2 μm SiO_2 insulation layer can be made from a silicon-on-insulator (SOI) substrate. According to the derived photonic band gap (PBG) diagram shown in Fig. 1, the ratio between the radius of the holes (r) and lattice constant (a) is selected as 0.341, where r and a are 140 nm and 410 nm, respectively. The normalized frequency range of photonic band gap extends from 0.262 to 0.320 in TM

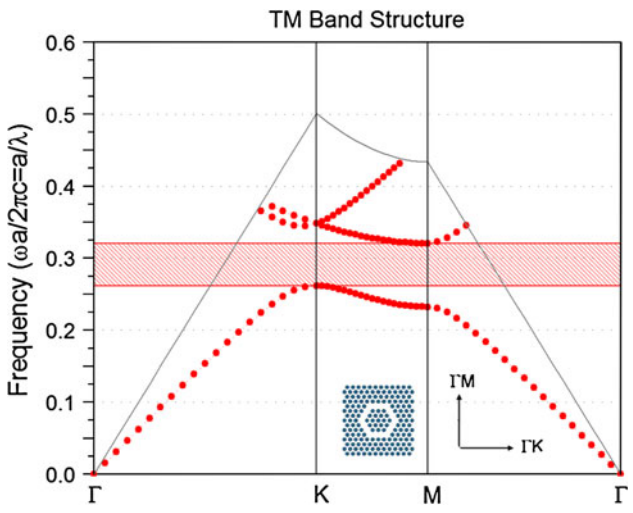

Fig. 1 Band structure of the PhCs structure of hexagonal lattice

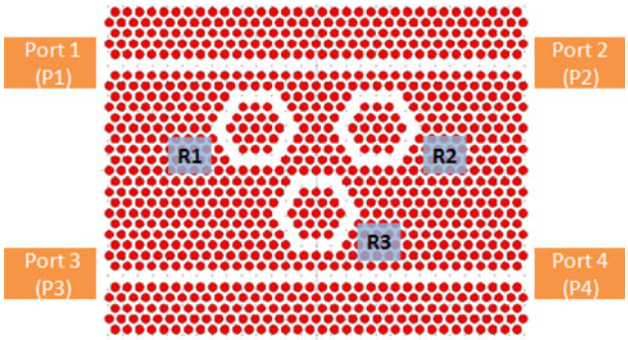

Fig. 2 Design of TNR resonator with its respective ports and coupling rings

polarization electromagnetic wave, i.e., the magnetic field parallel to the surface of silicon slab. The corresponding directions of ΓM and ΓK with respect to the hexagonal lattice are indicated in the inset of Fig. 1. Qiu (2002) reported a combinational approach of the 2-D finite-difference time-domain (FDTD) method and the effective refractive index (ERI) approximation. The data derived by this combinational approach are in good agreement with data given by the full vector three dimensional (3-D) FDTD method. This combinational approach was employed and the performance of the channel drop filter and the field distribution of the resonance mode of the TNR resonator were examined. As shown in the inset of Fig. 1, the resonance frequency of nano-ring resonator formed by removing holes of hexagonal trace is derived in the range of PBG. The ERI of water/220 nm-Si/SiO_2, i.e., the 220 nm silicon on a 2 μm SiO_2 slab, is calculated as 2.825 in the simulation, where the refractive index of water, SiO_2 and Si are 1.33, 1.46 and 3.46, respectively. The ERI of holes filled with water is 1.33. In this report, the refractive index change when various amount of biomolecules trapped in a specific hole is characterized as a shift of refractive index of that hole from 1.33 to 1.45 (Lee and Fauchet 2007). This is equivalent to trapping of an estimated mass of 1.5 fg of biomolecules in the sensing hole (Bennett et al. 1983).

Figure 2 shows the layout of the TNR resonator utilized in our design. Light can be launched into the resonator via one of the four ports. Through our careful selection of the radius and period, light from the input PhC waveguide is then coupled through the three rings (R1, R2 and R3) to the other side of the resonator, i.e., the opposite PhC waveguide. The output can then be measured from one of the two ports situated at the opposite PhC waveguide. For example, light can be input via Port 1 (P1) and after going through coupling by the rings, output can be obtained from Port 3 (P3) and Port 4 (P4). In this case, Port 2 (P2) will carry the "dropped" light. The output of such a scenario is shown in Fig. 3. The configuration of the TNR resonator is

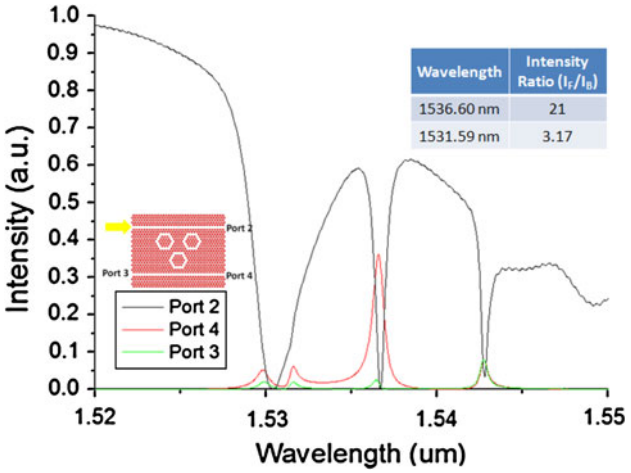

Fig. 3 Simulated spectra of three output ports when light is input via Port 1

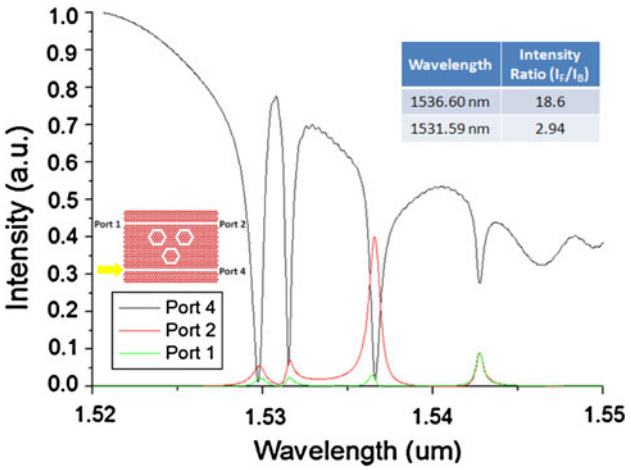

Fig. 4 Simulated spectra of three output ports when light is input via Port 3

shown in the inset, where the input light is indicated by a yellow arrow. In Fig. 3, Port 2 is defined as the transmission (TR) port, while Port 4 and Port 3 are denoted as the forward drop (FD) port and backward drop (BD) port respectively. It can be observed that a wavelength drop is exhibited at 1536.60 nm, where the intensity ratio of FD and BD signals is 21. This implies that a forward channel drop behavior has been obtained. In another configuration shown in Fig. 4, light is input at Port 3. Similar to the previous case, the wavelength drop is at 1536.60 nm, and the intensity ratio of Port 2 (FD) and Port 1(BD) signals is 18.6.

The fact that both configurations shown in Figs. 3 and 4 exhibit wavelength drop at the same wavelength is significant. With the asymmetrical arrangement of R1, R2 and R3, the resonance patterns when light is input via Port 1 and Port 3 are different. This is a representation of dual channel reversibility (DCR) which was reported by Li (Li and Lee 2011). In this work, we have managed to recreate such symmetrical output behavior in TNR resonator when it is placed in water instead of air by optimizing the ratio of the hole radius and lattice constant. The presence of DCR behavior opens the possibility of sensing multiple biomolecules at the same time and to corroborate the results. Both these features will be discussed more in depth in subsequent sections.

3 Bio sensing mechanism of TNR resonator

As shown in Fig. 2, the design of TNR resonator has four ports and hence there can be four different input/output arrangements. Due to the symmetrical layout of the TNR on the vertical axis, the case where light is input via Port 2 will yield the same output as the case where light is input via Port 1. Similarly, the output produced when light is input via Port 4 will be the identical to the output when light is input via Port 3. This means that from four different input/output arrangements, we can reduce to two cases which are summarized in Fig. 5. For the other two arrangements, they will only be utilized in Sect. 4 where they are used as a corroboration mechanism. Based on Figs. 3 and 4, it was established that in both case 1 and case 2, only the FD port output is important as it shows significant increase in intensity at 1536.60 nm.

Despite having similar outputs, continuous wave (CW) resonance patterns of case 1 and case 2 are significantly different from each other. This means that multiple molecules can be sensed simultaneously by carefully selecting specific holes to be used for bio sensing. In Fig. 6, the CW resonance pattern of case 1 with an input wavelength of 1536.60 nm is shown. There are a total of six frames which show the resonance that happen at six transit time points within the TNR resonator. Light is launched into the TNR resonator from Port 1. Energy is coupled into R1, while a significantly smaller proportion is coupled into R2. The energy in R2 is found to be transferred to R1 and jointly the energy in R1 is moved to R3 as shown in Fig. 6a, b. While some energy in R3 is noticed to be transferred back to R2, most of the energy is coupled to the FD port at Port 4, shown in Fig. 6c. Figure 6d–f show similar scenarios as Fig. 6a–c expect that they are 180° out of phase, thus completing one period of the wave.

In Fig. 7, the CW resonance pattern of case 2 with a similar input wavelength of 1536.60 nm is illustrated. A total of six frames to show the resonance pattern at six transit times are also captured to help visualize the resonance within the TNR resonator. Light is input at Port 3 and most of the energy is found to be coupled into R3, shown in Fig. 7a. The energy is then found to be

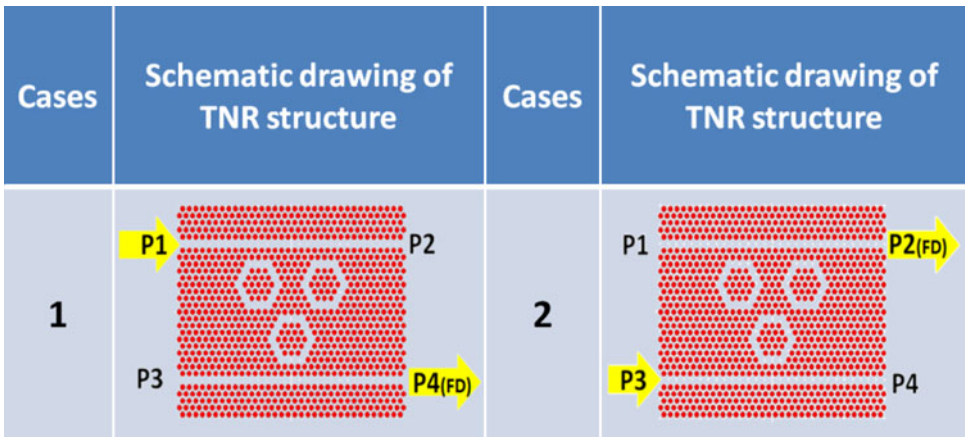

Fig. 5 Different cases where light can be input into the TNR resonator

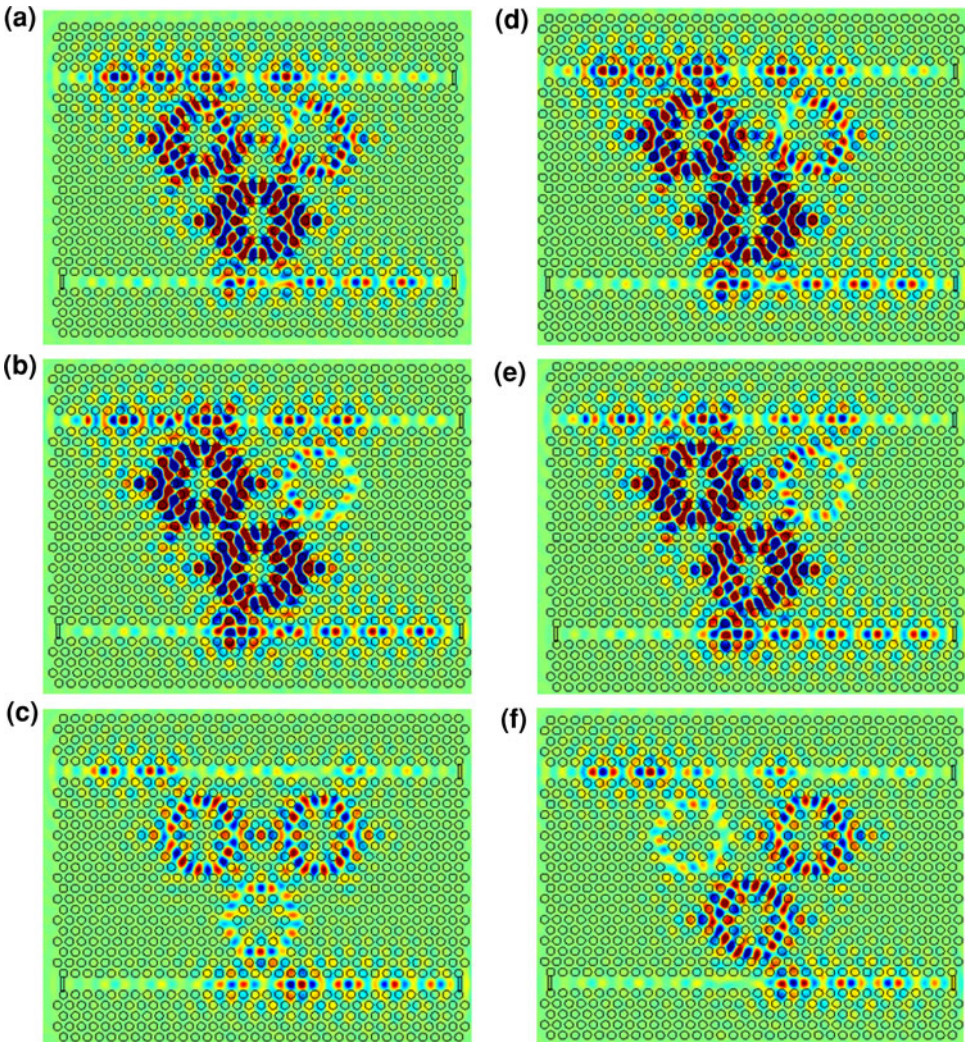

Fig. 6 Images of continuous wave field distribution for TNR resonators when light is input via Port 1

distributed to R2. From R2, the energy shows two different behaviors. A small proportion of the energy is coupled into R1, which are then looped back into R3, as illustrated in Fig. 7b, c. Majority of the energy in R2 is coupled into the output waveguide and are transferred to the FD port at Port 3. Figure 7d–f depict the same scenarios with the wave 180° out of phase and this completes the period.

From Figs. 6 and 7, we can observe similar trend of energy exchange within the three rings. It is discovered that only two rings, either one of the upper rings, R1 or R2, and

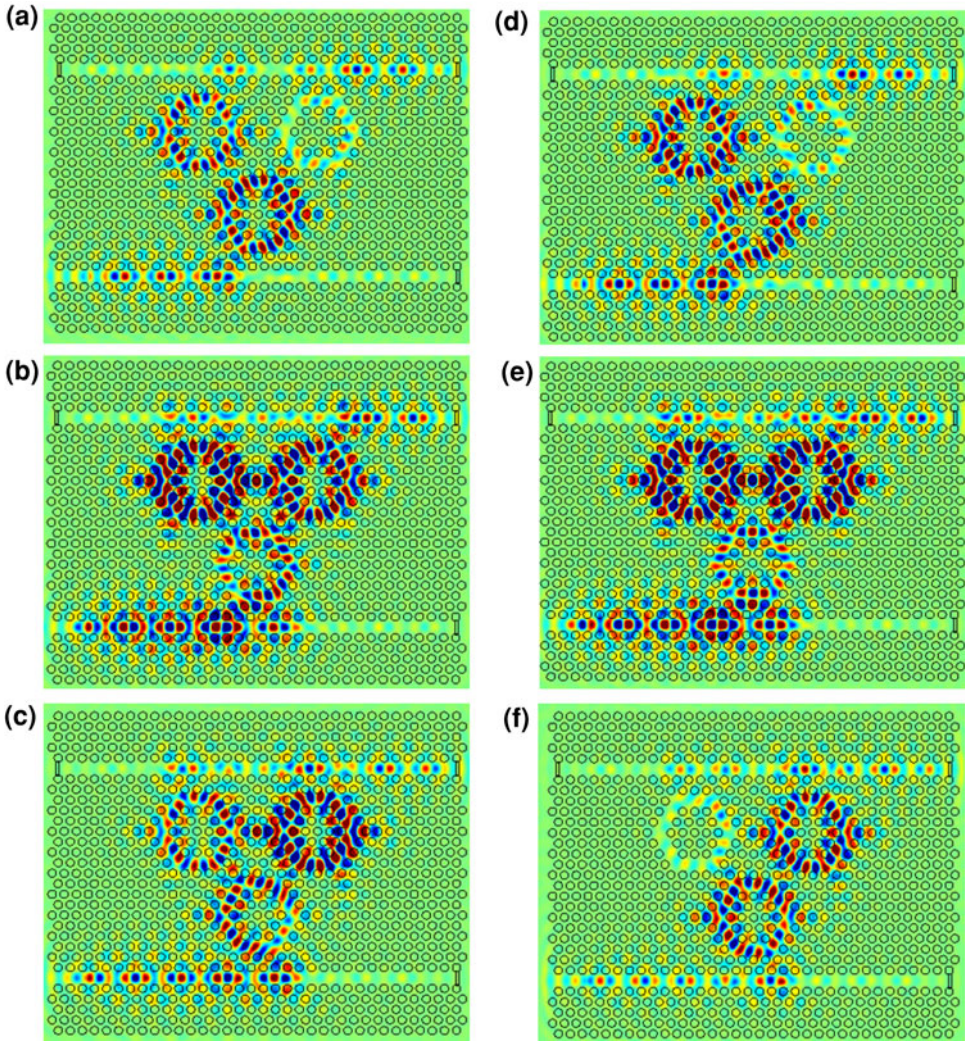

Fig. 7 Images of continuous wave field distribution for TNR resonators when light is input via Port 3

the bottom ring R3, play important roles in the main energy transfer from the input waveguide to the output waveguide. The resonance modes that occur in both cases contribute energy mainly to the FD port, which explains why the TNR resonator displays the channel drop filter behavior. In both case 1 and case 2 in Fig. 5, we are able to observe similar trend in the resonance modes, especially in the rings that coupled the energy to the output waveguide. However, the field distributions between the two cases display some distinctions. The combination of these two factors gives explanation on the appearance of similar drop wavelength but at different output intensities.

The different energy exchange scenario in both cases is significant in the application of TNR resonator as biosensor. In case 1, energy exchange mainly occur within R1 and R3 and hence the spectra output is very sensitive to changes of the refractive index near R1. The main energy exchange for case 2 takes place largely in R2 and R3 and this causes the spectra output of case 2 to be highly sensitive to changes of the refractive index near R2. In order to exemplify this, we have chosen certain holes, as shown in Fig. 8, to be used as sensing holes.

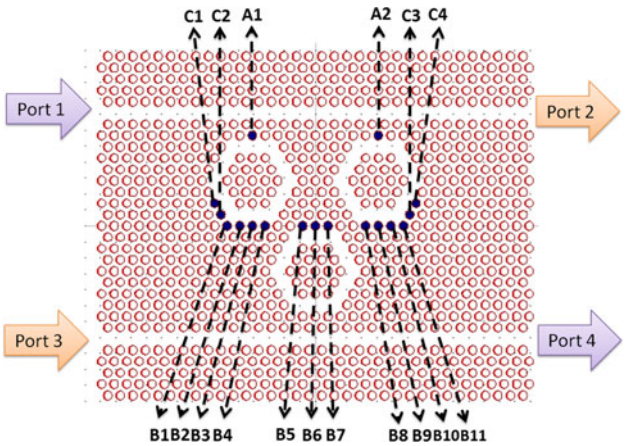

Fig. 8 Locations and identification of sensing holes used

Detection of biomolecules is depicted by the scenario where a minute amount of the target biomolecules flow in a

fluidic channel and are brought through the sensing hole. The target biomolecules are then bound to the sensing hole through the use of selective binding mechanism, for example, using antigen to antibody or DNA probe to DNA. When the biomolecules are maneuvered into the respective holes one by one, the refractive index of the sensing hole is changed locally. As mentioned, this change is characterized by changing the refractive index of the hole from 1.33 to 1.45, where the refractive index of 1.45 represents the situation that the hole is fully occupied by biomolecules. Consequently, this induces a red shift in the FD peak when light is input at Port 1 and Port 3 separately. One such case is depicted in Fig. 9 where the sensing of biomolecules that is trapped at B3 using case 1. The reference curve shows the output when there is no immobilization of biomolecules into the sensing hole. As illustrated, when a biomolecule is bound in the sensing hole, a red shift of 0.22 nm in the FD peak occurs due to the changes in refractive index in that hole. Similar simulations are done to the other sensing holes and the resultant forward drop peak shifts are recorded and summarized in Fig. 10. It can be observed that certain points show a FD peak shift when light is input from either Port 1 or Port 3. Considering case 1 where light is input via Port 1, the forward drop peak shift induced for sensing holes B1–B4 and C1–C2 are expected since the CW resonance pattern shows that the output spectra is most sensitive to refractive index changes near R1. The fact that no significant FD peak shift is observed when sensing holes B8–B11 and C3–C4 are utilized can also be anticipated as according to the CW resonance pattern, refractive index changes near R3 have little impact. Similar scenario is found for the results in case 2 where light is input via Port 3. It is found that FD peak shift is only induced for changes in refractive index in sensing holes B8–B11 and C3–C4. However, similar red shift in FD peak is not found when

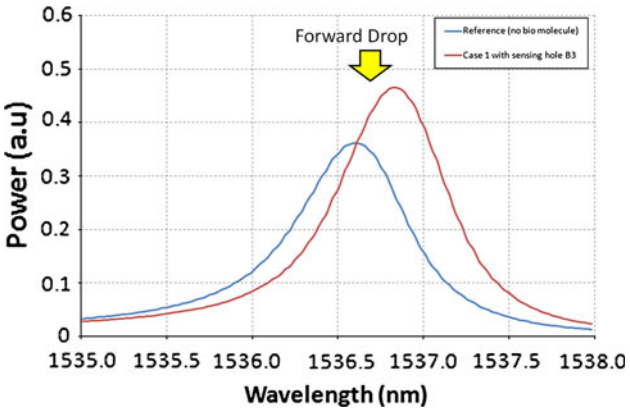

Fig. 9 Spectra of forward drop peak of reference and output when sensing hole B3 is used

using sensing holes B1–B4 and C1–C2. This is in agreement with our discussion regarding the CW resonance pattern where a refractive change near R2 is vital in inducing red shift in the FD peak. While most of the outputs due to the binding of biomolecules to the sensing holes are anticipated, it has to be noted that wavelength shifts occurring because of the changes in B5 and B7 do not follow the general trend. Instead of following the inclination of having significant FD peak shift in R1 for case 1 and R2 for case 2, the resulted peak shift is zero for sensing hole B5 in case 1 and B7 in case 2. This phenomenon can be explained upon closer inspection of the CW resonance pattern. Considering case 1, when light is coupled from R1 to R3, energy that is coupled into B5 is found to be travelling back into R1 instead. This cancels the effect of the refractive index change which would have induced the forward drop peak shift. This is similar in case 2. When light is travelling from R3 to R1, the energy coupled into B7 is found to be travelling back into R3 instead.

Fig. 10 Simulation results of forward drop peak shift when biomolecule is bound to the different sensing holes

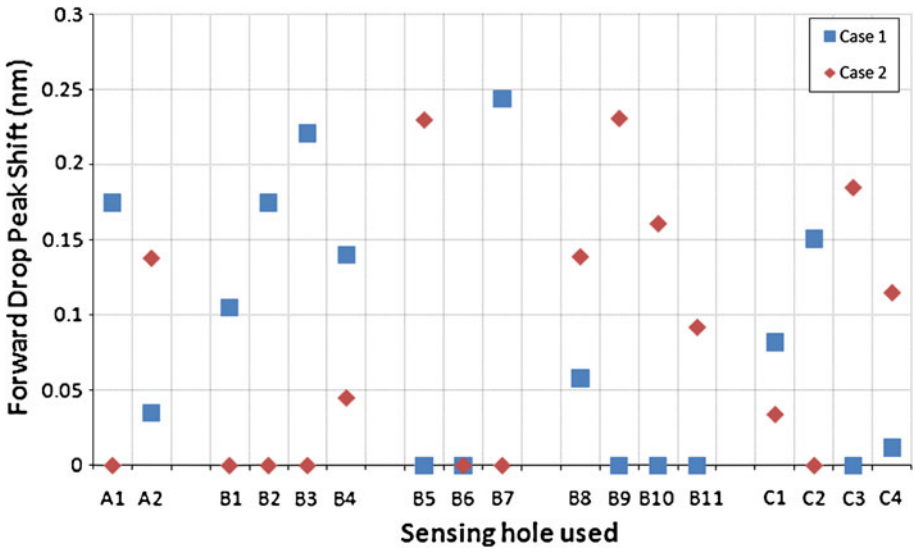

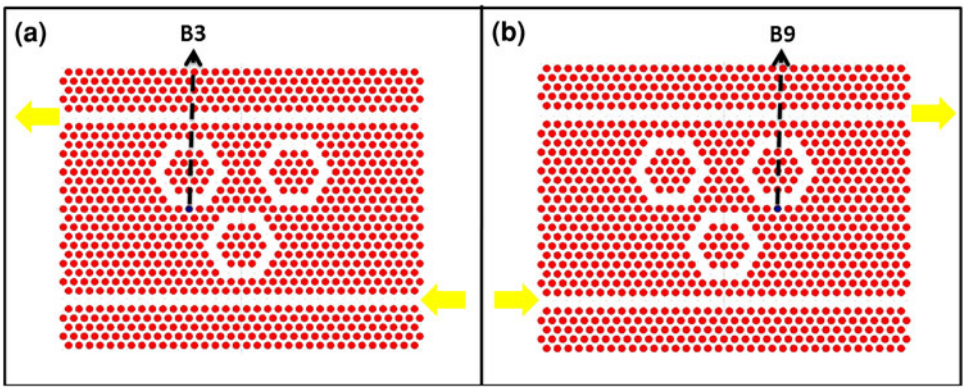

Fig. 11 **a** Schematic of layouts when sensing B3 using Port 4 as input. **b** The equivalent layout of (**a**) by sensing B9 using case 2

From Fig. 10, we are also able to identify sensing holes that induces FD peak shift for only either case 1 or case 2, but not both. For example, when a biomolecule is bound to B3, a red shift is induced only when light is input from Port 1. On the other hand, for biomolecules bound to B9, a red shift is only observed when light is launched from Port 3. This indicates that the FD peak shifts due to these holes are independent of each other. Light can be input into Port 1 and Port 3 separately, while outputs are measured at Port 2 and Port 4, and the resultant shift in FD peaks at corresponding output ports are dictated by the sensing holes where the biomolecules are trapped. By harnessing the independence relationship of the sensing holes on the FD peak shift, multiple sensing of biomolecules at the same input frequency is hence made possible.

The performance of the TNR resonator as a biosensor offers much optimism. Compared to DNR resonator biosensor counterpart, the amount of red shift of the FD peak in the most sensitive sensing hole is found to have increase from 0.18 to 0.24 nm (Hsiao and Lee 2011), which is an improvement of 33 %. When multiple biomolecules sensing are desired in DNR resonator biosensor, it has to be noted that the most sensitive sensing holes cannot be used. This limitation is not present in TNR resonator biosensor. As the FD peak shifts due to the different sensing holes are independent of each other, the sensing holes that induce the highest red shifts in FD peak can be used.

4 Corroboration mechanism

An additional advantage of TNR resonator to be used as biomolecule sensing device is that it has the ability to do corroboration. For example, we have established that sensing hole B3 induces a FD peak shift of 0.22 nm when light is input via Port 1. Corroboration of this result can be made by inputting light via Port 4. Due to the symmetry of the TNR resonator along the horizontal plane, an input via Port 4 would yield similar results as an input via Port 3 except that the output forward drop peak shift is now reversed. When light is input via Port 4 to cross-check the result obtained for biomolecule bonded to B3, as shown in Fig. 11a, it will produce the same results as case 2 with Port 3 as the input detecting the biomolecule in sensing hole B9, as shown in Fig. 11b. This will produce a red shift of 0.23 nm in the FD peak. This means that for every sensing hole, there are two different FD peak shifts that are associated with it. Given that the shifts in peak in such application are typically very small, such methods are of paramount importance to ascertain that the results obtained are accurate and correct. In addition, one unique characteristic of the corroboration mechanism is that by choosing sensing holes carefully, as of the case of using B3, we are able to utilize the more significant and larger shifts in forward drop peak for both the sensing and corroboration processes. This process helps to make certain of the results that are obtained using case 1 and case 2. By leveraging the symmetrical nature of the TNR resonator, such applications are only possible through the fact that the peak shift induced due to the changes in the sensing holes in one case is independent of that in the other cases. In other words, these cases do not cause interference.

5 Conclusion

We have proposed a novel silicon PhCs based TNR resonator with the ability to be implemented in biomolecules sensing. A strong peak at 1536.60 nm which is derived at forward drop (FD) port points out that the TNR resonator is a good channel drop filter. When a biomolecule is bound to a sensing hole in the TNR resonator, it changes the refractive change and this induces a forward drop peak shift which can be measured. We have explained and predicted how the shift is induced by examining the nature of distributed magnetic field of the CW resonance patterns. The amount of red shift when different sensing holes are used has been simulated and consolidated, and it is found out that the performance of such a TNR resonator biosensor outperforms its DNR resonator biosensor counterpart by up

to 33 %. In addition, we have also discovered that the forward drop peak shifts due to certain sensing holes are highly dependent on the port where the light is input. For instance, for sensing holes like B3 and B9, FD peak shift are only induced when light is input via either Port 1 or Port 3 but not both. This makes the peak shifts of the two cases independent of each other. A major application of this feature is that it allows the sensing of multiple biomolecules at the same input frequency through the use of appropriate sensing holes. The non-interfering nature of the sensing capability of each sensing hole also ensures that we are able to select the more sensitive sensing holes, which offer the most red shift in FD peak, when multiple biomolecule sensing is implemented. In addition, by exchanging the input and output ports, we are able to implement the corroboration mechanism. As changes in the peak location in such biomolecule sensing application are usually minute, this feature helps to ascertain the presence of biomolecules. This trait makes the TNR resonator to be an even more suitable candidate for such highly sensitive biomolecule sensing.

Acknowledgments This work was supported in research grant of Academic Research Committee Fund MOE2009-T2-2-011 (R-263000598112) at the National University of Singapore, and A*-STAR, SERC Grant Nos. 0921010049, 1021010022 and 1021650084.

References

Bennett MD, Heslop-Harrison JS, Smith JB, Ward JP (1983) DNA density in mitotic and meiotic metaphase chromosomes of plants and animals. J Cell Sci 63:173–179

Djavid M, Monifi F, Ghaffari A, Abrishamian MS (2008) Heterostructure wavelength division demultiplexers using photonic crystal ring resonators. Optics Commun 281:4028–4032

Hsiao F-l, Lee C (2010) Computational study of photonic crystals nano-ring resonator for biochemical sensing. Sensors J IEEE 10:1185–1191

Hsiao F-L, Lee C (2011) Nanophotonic biosensors using hexagonal nanoring resonators: computational study. J Micro/Nanolithogr MEMS MOEMS 10:013001–013008

Hung-Ta C, Chengkuo L, Hua-Kung C, Kuei-Chu H, Chii-Chang C, Ho JAA, Chien C (2009) The comparison between the graded photonic crystal coupler and various couplers. J Lightw Techol 27:2570–2574

Intonti F, Vignolini S, Riboli F, Zani M, Wiersma DS, Balet L, Li LH, Francardi M, Gerardino A, Fiore A, Gurioli M (2009) Tuning of photonic crystal cavities by controlled removal of locally infiltrated water. Appl Phys Lett 95:173112–173113

Iqbal M, Gleeson MA, Spaugh B, Tybor F, Gunn WG, Hochberg M, Baehr-Jones T, Bailey RC, Gunn LC (2010) Label-free biosensor arrays based on silicon ring resonators and high-speed optical scanning instrumentation. J Sel Topics Quantum Electron IEEE 16:654–661

Kirk JT, Fridley GE, Chamberlain JW, Christensen ED, Hochberg M, Ratner DM (2011) Multiplexed inkjet functionalization of silicon photonic biosensors. Lab Chip 11:1372–1377

Kitamura M, Iwamoto S, Arakawa Y (2005) Enhanced light emission from an organic photonic crystal with a nanocavity. Appl Phys Lett 87:151119–151123

Lalanne P, Sauvan C, Hugonin JP (2008) Photon confinement in photonic crystal nanocavities. Laser Photonics Rev 2:514–526

Lee MR, Fauchet PM (2007) Two-dimensional silicon photonic crystal based biosensing platform for protein detection. Opt Express 15:4530–4535

Lee C, Thillaigovindan J (2009) Optical nanomechanical sensor using a silicon photonic crystal cantilever embedded with a nanocavity resonator. Appl Opt 48:1797–1803

Lee C, Radhakrishnan R, Chii-Chang C, Jing L, Thillaigovindan J, Balasubramanian N (2008) Design and modeling of a nanomechanical sensor using silicon photonic crystals. J Lightw Technol 26:839–846

Li B, Lee C (2011) NEMS diaphragm sensors integrated with triple-nano-ring resonator. Sens Actuators A 172:61–68

Li B, Hsiao F-L, Lee C (2011a) Computational characterization of a photonic crystal cantilever sensor using a hexagonal dual-nanoring-based channel drop filter. IEEE Trans Nanotechnol 10:789–796

Li B, Hsiao F-L, Lee C (2011b) Configuration analysis of sensing element for photonic crystal based NEMS cantilever using dual nano-ring resonator. Sens Actuators A 169:352–361

Lu T-W, Lin P-T, Sio K-U, Lee P-T (2010) Optical sensing of square lattice photonic crystal point-shifted nanocavity for protein adsorption detection. Appl Phys Lett 96:213702–213703

Mai TT, Hsiao F-L, Lee C, Xiang W, Chen C–C, Choi WK (2011) Optimization and comparison of photonic crystal resonators for silicon microcantilever sensors. Sens Actuators A 165:16–25

Monifi F, Ghaffari A, Djavid M, Abrishamian MS (2009) Three output port channel-drop filter based on photonic crystals. Appl Opt 48:804–809

Qiang Z, Zhou W, Soref RA (2007) Optical add-drop filters based on photonic crystal ring resonators. Opt Express 15:1823–1831

Qiu M (2002) Effective index method for heterostructure-slab-waveguide-based two-dimensional photonic crystals. Appl Phys Lett 81:1163–1165

Saghirzadeh Darki B, Granpayeh N (2010) Improving the performance of a photonic crystal ring-resonator-based channel drop filter using particle swarm optimization method. Optics Commun 283:4099–4103

Vahala KJ (2003) Optical microcavities. Nature 424:839–846

Vos KD, Girones J, Claes T, Koninck YD, Popelka S, Schacht E, Baets R, Bienstman P (2009) Multiplexed antibody detection with an array of silicon-on-insulator microring resonators. IEEE Photonics J 1:11

Zhang Z, Qiu M (2005) Compact in-plane channel drop filter design using a single cavity with two degenerate modes in 2D photonic crystal slabs. Opt Express 13:2596–2604